ChemComm

COMMUNICATION

View Article Online
View Journal | View Issue

Cite this: *Chem. Commun.*, 2024, **60**, 9093

Received 3rd March 2024,
Accepted 22nd July 2024

DOI: 10.1039/d4cc01023j

rsc.li/chemcomm

High-area alumina supported Cu–Ce atomic species for water–gas shift reaction†

Yiwei Yu,[a] Tie Wang,[bc] Ning Yan [b] and Jingyue Liu *[d]

Atomically dispersed cerium species, anchored to high-area alumina by unsaturated penta-coordinated aluminum, strongly interact with atomically dispersed Cu species to provide active centers for water–gas shift reaction (WGSR). The alumina-anchored Ce^{3+} species stabilize atomically dispersed Cu^{+} to form Cu^{+}–Ce^{3+} active complexes and they work synergistically to enhance low-temperature WGSR activity. This work offers alternative approaches to developing low-cost catalysts for the WGSR process.

The water–gas shift reaction (WGSR) is a highly valuable industrial process for manufacturing hydrogen, ammonia, methanol, and hydrocarbons. For example, WGSR plays an important role in the production of hydrogen *via* steam reforming of methane or other types of hydrocarbons.[1] The copper–ceria catalytic system has exhibited remarkable efficiency in low-temperature WGSR.[2,3] The strong interaction between copper species and the ceria support, leading to modifications of the copper chemical state at the copper–ceria interfaces, is considered to be key to the notable catalytic performance.[4,5] The perimetric boundaries between copper particles and crystalline ceria support surfaces are proposed to be the active centers for WGSR.[5,6]

Anchored metal atoms, due to their strong interaction with the support, function as effective active centers for a variety of catalytic reactions,[7] including WGSR.[8] Recently, atomically dispersed Cu species, supported on crystalline CeO_2, demonstrated higher activity than copper clusters/particles for WGSR, primarily due to strong interactions between atomic copper and selected facets of crystalline ceria.[9] Specifically, the CeO_2 {111} facets stabilize more atomically dispersed copper species, and therefore increase the number of active sites for low-temperature WGSR.[9] Such strong electronic interactions between Cu atoms/clusters and surface Ce^{3+} species on crystalline CeO_2 maintain stable Cu^{+} species during the WGSR.[5] The interfacial Cu^{+}–O_V–Ce^{3+} complexes are considered to serve as active sites, where the Cu^{+} adsorbs a CO molecule and the neighboring O_V–Ce^{3+} site dissociatively activates H_2O.[5] The adsorbed CO is either oxidized by a reactive oxygen on the CeO_2 surface to form a CO_2 or it reacts with surface OH groups to form an intermediate which subsequently decomposes to H_2 and CO_2.[10–12] Abundant surface OH groups from water dissociation and their intimate contacts with adsorbed CO molecules at the copper–ceria interfaces are critical to high WGSR activity.[13] It is not clear whether crystalline CeO_2 is required for developing highly active Cu-based catalysts for low-temperature WGSR.

In this work, we demonstrate that atomically dispersed Ce species not only stabilize atomically dispersed Cu but also modify their electronic structure to form stable Cu^{+}–Ce^{3+} active centers that significantly enhance the activity of low-temperature WGSR. Commercially available, high-area γ-Al_2O_3 was used to support the atomically dispersed metal species. Experimental results showed that atomically dispersed Ce atoms have a major effect on the catalytic behavior of atomically dispersed Cu species: the grafting of Ce atoms onto γ-Al_2O_3 surfaces increased the WGSR rate of Cu atoms by nine times at a reaction temperature of 200 °C. The WGSR activity of the atomically dispersed Cu–Ce/γ-Al_2O_3 catalyst, with Cu and Ce loading levels of only 1.2 wt% and 2.2 wt%, respectively, is comparable to that of the Cu/CeO_2 catalysts reported in the literature.[9,14] We propose that the intimate contact between Cu and Ce atoms induces strong electronic interaction and the Cu–Ce species act synergistically to provide enhanced WGSR activity: the Ce^{3+} adsorbs and dissociates H_2O whereas the adjacent Cu^{+} adsorbs CO. The activated OH species react with the CO molecules on the Cu^{+} sites, which are stabilized by neighboring Ce^{3+}, forming intermediate species and subsequently decomposing to CO_2 and H_2.

[a] *School for Engineering of Matter, Transport and Energy, Arizona State University, Tempe, Arizona 85287, USA*
[b] *Department of Chemical and Biomolecular Engineering, National University of Singapore, Singapore 117585, Singapore*
[c] *Joint School of NUS and TJU, International Campus of Tianjin University, Fuzhou 350207, China*
[d] *Department of Physics, Arizona State University, Tempe, Arizona 85287, USA. E-mail: Jingyue.liu@asu.edu*

† Electronic supplementary information (ESI) available. See DOI: https://doi.org/10.1039/d4cc01023j

An electrostatic-adsorption-assisted deposition method was used to disperse the Ce and Cu species onto high-area γ-Al_2O_3 (see ESI† for details). The content of the Cu and Ce in the as-synthesized Cu–Ce/γ-Al_2O_3 catalyst was measured to be 1.2 wt% and 2.2 wt%, respectively. Catalysts with lower Cu content were synthesized and evaluated as well (Table S1, ESI†). Cu/γ-Al_2O_3, containing 1.4 wt% of atomically dispersed Cu species, was synthesized as a control catalyst. The XRD patterns of the Cu/γ-Al_2O_3 and Cu–Ce/γ-Al_2O_3 catalysts (Fig. S1, ESI†) did not provide recognizable diffraction peaks of Ce- or Cu-related crystalline phases. Although low levels of metal loading complicate the interpretation of the XRD patterns, these catalysts did not contain large crystals of Ce and Cu compounds as evidenced by SEM and STEM examinations.

Because of its high sensitivity to particles of heavy elements, the backscattered electron (BSE) imaging method was used to screen the catalyst samples to optimize our synthesis processes (Fig. S2, ESI†). BSE images of the Cu–Ce/γ-Al_2O_3 (Fig. S2(c and d), ESI†) and Cu/γ-Al_2O_3 (Fig. S3(a and b), ESI†) catalysts show the absence of large particles/agglomerates of Cu- or Ce-containing species. High-angle annular dark-field (HAADF) images, which provide atomic number (Z) contrast, of the Cu/γ-Al_2O_3 catalyst show the absence of Cu particles/clusters (Fig. S4a, ESI†) and the presence of atomically dispersed Cu species (Fig. S4b and c, ESI†). A representative HAADF image of the Cu–Ce/γ-Al_2O_3 catalyst (Fig. 1a) confirms the absence of detectable Cu-/Ce-related particles. The atomic-resolution HAADF image (Fig. 1b) unambiguously shows the spatial distribution of the atomically dispersed Ce and Cu atoms on the γ-Al_2O_3 support. Reliable information on the elemental mapping of individual Ce and Cu atoms is beyond the current instrumentation limit.[15]

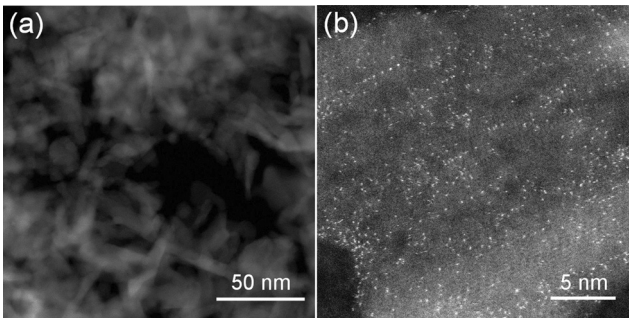

Fig. 1 (a) Representative low-magnification HAADF-STEM image of Cu–Ce/γ-Al_2O_3 showing the absence of metal clusters/particles. (b) Representative atomic resolution HAADF-STEM image displaying atomically dispersed metal species uniformly distributed on the γ-Al_2O_3 support. Atomically dispersed Cu atoms could not be reliably distinguished from the Ce single atoms.

The X-ray photon spectroscopy (XPS) method was used to characterize atomically dispersed Cu/Ce species in the reduced (300 °C for 1 h in 5 vol% H_2/He) Cu/γ-Al_2O_3 and Cu–Ce/γ-Al_2O_3. The wide-scan spectra of Cu/γ-Al_2O_3 and Cu–Ce/γ-Al_2O_3 (Fig. S5, ESI†) indicate the presence of Cu, O, C and Al in both catalysts and Ce in the Cu–Ce/γ-Al_2O_3 catalyst. The Ce 3d XPS spectrum of the Cu–Ce/γ-Al_2O_3 (Fig. 2a) shows all the characteristic peaks (v_0, v', u_0, and u') of Ce^{3+} species and absence of the peaks representing Ce^{4+} species,[16] in agreement with literature reports.[17–19] The Cu 2p XPS spectra of the Cu/γ-Al_2O_3 and Cu–Ce/γ-Al_2O_3 catalysts (Fig. 2b) show peaks at 932.7 eV and 952.4 eV, corresponding to Cu $2p_{3/2}$ and Cu $2p_{1/2}$, respectively.[20] The Cu $2p_{3/2}$ peak can be deconvoluted into two distinct peaks: Cu^{2+} at 933.8 eV and Cu^0/Cu^+ at 932.4 eV.[20] The Cu Auger LMM region (Fig. S6, ESI†) suggests characteristic peaks of Cu^+ and Cu^{2+} but not the characteristic peaks of the Cu^0 species.[20] The percentage of Cu^+ to the total Cu species (Cu^+ + Cu^{2+}) was estimated to be ~57% in the Cu/γ-Al_2O_3 and ~82% in the Cu–Ce/γ-Al_2O_3.

We conducted *in situ* diffuse reflectance infrared Fourier transform (DRIFT) experiments to study the dynamic behaviour of CO adsorption on the metal species. All catalysts were first pre-treated in H_2 at 300 °C for 1 h, then CO molecules were allowed to adsorb on the metal species at 25 °C to saturation, and finally the CO desorption experiment was carried out with flowing argon (Fig. S7, ESI†). Fig. 2c displays the CO absorption spectra after argon purging: no detectable CO adsorption on Ce/γ-Al_2O_3 and a distinct IR band at 2108 cm^{-1} on the

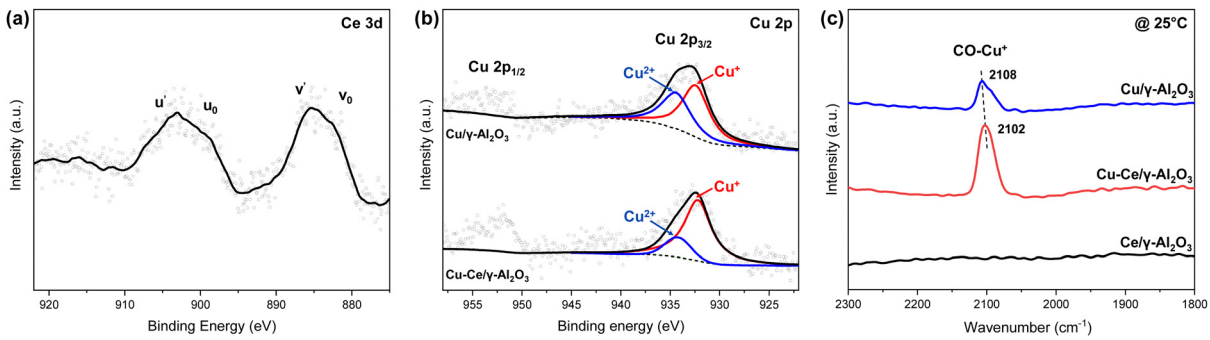

Fig. 2 The XPS spectrum of the Ce 3d region of Cu–Ce/γ-Al_2O_3 (a) clearly reveals characteristic peaks of the Ce^{3+} species and XPS spectra of the Cu 2p region of Cu/γ-Al_2O_3 and Cu–Ce/γ-Al_2O_3 (b) show higher Cu^+ content in Cu–Ce/γ-Al_2O_3. Catalysts were reduced at 300 °C in 5 vol% H_2/He for 1 h prior to the acquisition of the XPS spectra. *In situ* DRIFT spectra of CO adsorption at 25 °C on Ce/γ-Al_2O_3, Cu/γ-Al_2O_3, and Cu–Ce/γ-Al_2O_3 (c) show no CO adsorption on Ce/γ-Al_2O_3 and CO adsorption on the Cu^+ sites in Cu/γ-Al_2O_3 and Cu–Ce/γ-Al_2O_3. Prior to the CO adsorption–desorption experiment, all catalysts were reduced by 5% H_2 at 300 °C for 1 h. The spectra were collected after 60 min purging with Ar for Cu/γ-Al_2O_3 and Cu–Ce/γ-Al_2O_3, and 20 min purging with Ar for Ce/γ-Al_2O_3.

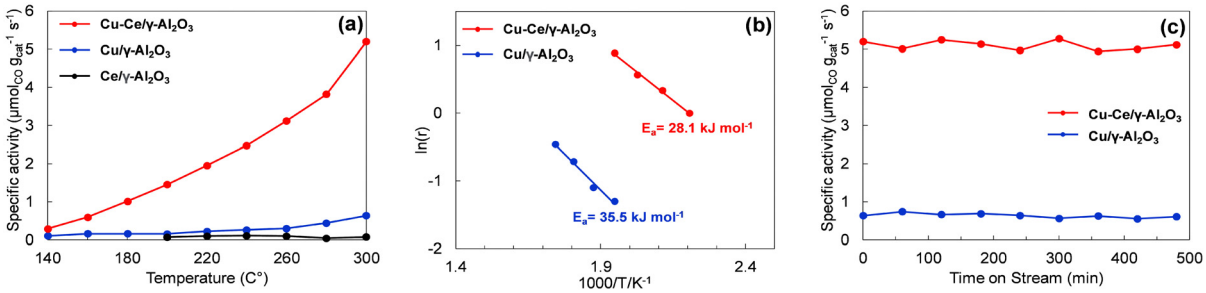

Fig. 3 Plots of WGSR specific activity *vs.* temperature over Ce/γ-Al_2O_3, Cu/γ-Al_2O_3, and Cu–Ce/γ-Al_2O_3 catalysts (a) clearly show significantly enhanced activity of the Cu–Ce/γ-Al_2O_3 catalyst. Arrhenius plots for WGSR over Cu/γ-Al_2O_3 and Cu–Ce/γ-Al_2O_3 (b). Long-term stability tests over Cu/γ-Al_2O_3 and Cu–Ce/γ-Al_2O_3 catalysts at 300 °C (c) demonstrate the stability of both catalysts during low-temperature WGSR. Reaction conditions: 1% CO + 10% H_2O + He balance, SV = 74 400 ml g^{-1} h^{-1}. The Cu–Ce/γ-Al_2O_3 catalyst contains 1.2 wt% Cu and 2.2 wt% Ce; the Cu/γ-Al_2O_3 catalyst contains 1.4 wt% Cu.

Cu/γ-Al_2O_3, assignable to linear CO adsorption on single Cu^+ species.[21,22] The red-shifted, prominent band at 2102 cm^{-1} on the Cu–Ce/γ-Al_2O_3 catalyst demonstrates strong Cu^+ interaction with Ce^{3+} species.[23,24]

It has been reported that under oxidative conditions, atomically dispersed Cu species maintain a +2 valence state while under reducing conditions some of the anchored Cu^{2+} species can be reduced to Cu^+.[25] However, variations in the reducibility of copper species in the Cu/γ-Al_2O_3 catalyst have been reported.[25,26] Previous studies showed that the atomically dispersed Cu^{2+} species in a 0.5 wt% CuO/γ-Al_2O_3 catalyst could not be reduced in H_2 at temperatures up to 700 °C.[26] Some of the strongly anchored Cu^{2+} species in our Cu/γ-Al_2O_3 catalyst might not have been reduced after the mild reduction treatment in H_2 at 300 °C. The increased amount of Cu^+ species in the reduced Cu–Ce/γ-Al_2O_3 catalyst suggests that the atomically dispersed Ce^{3+} species facilitated the reduction of the Cu species, in agreement with those reported in the literature.[17,27–29] Our XPS and DRIFTS results confirmed that the presence of alumina-anchored Ce^{3+} species increased the amount of Cu^+ species after mild H_2 reduction at 300 °C. Modification of the alumina support may increase the maximum loading level of the atomic Ce species and subsequently enhances the number of active Cu^+ species in the reduced Cu–Ce/γ-Al_2O_3 catalyst.

The CO conversion (Fig. S8, ESI†) and the specific reaction rates (Fig. 3a) as a function of temperature over the Ce/γ-Al_2O_3, Cu/γ-Al_2O_3 and Cu–Ce/Al_2O_3 catalysts show that at WGSR temperatures $\leq$ 300 °C, the Ce/γ-Al_2O_3 (2.2 wt% Ce) did not convert much CO at all. The Cu–Ce/γ-Al_2O_3 (~1.2 wt% Cu and 2.2 wt% Ce), on the other hand, gave a reaction rate of 1.4 μmol_{CO} g_{cat}^{-1} s^{-1} at 200 °C, about nine times higher than that (1.6×10^{-1} μmol_{CO} g_{cat}^{-1} s^{-1}) over the Cu/Al_2O_3 (~1.4 wt% Cu) control catalyst. Kinetic experiments (Fig. 3b) showed an apparent activation energy (E_a) of 28.1 kJ mol^{-1} for WGSR on the Cu–Ce/γ-Al_2O_3, much lower than the 35.5 kJ mol^{-1} of the Cu/γ-Al_2O_3. The impact of possible residue Na ions in the Cu–Ce/γ-Al_2O_3 catalyst on the WGSR activity was negligible (Fig. S9, ESI†). The fact that the specific activity of WGSR almost linearly increases with the total number of Cu atoms in the Cu–Ce/γ-Al_2O_3 catalysts (Fig. S10, ESI†) suggests that the Cu species were most probably atomically dispersed or isolated from each other. The activity of the atomically dispersed Cu–Ce/γ-Al_2O_3 catalyst is comparable to those of the CeO_2 supported Cu catalysts (Table S2, ESI†). Our atomically dispersed Cu–Ce/γ-Al_2O_3 catalyst, however, contained only 2.2 wt% Ce and 1.2 wt% Cu, significantly lower than those of the traditional Cu/CeO_2 catalysts reported in the literature. The long-term WGSR tests at 300 °C (Fig. 3c) showed that both the Cu/Al_2O_3 and Cu–Ce/γ-Al_2O_3 catalysts were stable. Atomic resolution HAADF images of the used Cu/γ-Al_2O_3 (Fig. S11, ESI†) and Cu–Ce/γ-Al_2O_3 (Fig. S12, ESI†) catalysts (after 8 hours of continuous WGSR reaction) did not show sintering of the atomically dispersed Cu and Ce species.

Isolated Cu^+ sites are active for CO adsorption.[9,25,30,31] On reducible oxides, water adsorption/dissociation is generally considered to occur on the neighboring sites of the Cu^+ species (*i.e.* Ti^{3+}, Ce^{3+}–O_v, Cu^0);[9,30–32] competitive adsorption of both CO and H_2O molecules, and slow H_2O dissociation, on individually isolated Cu^+ sites pose limitations on the WGSR on atomically dispersed Cu/γ-Al_2O_3 catalysts.[33] Experimental and computational results revealed that single Ce atoms adsorb water molecules and facilitate their dissociation process.[34,35] Furthermore, the electronic interaction between highly active Ce species and transition metals might modulate the adsorption strength of intermediate species and expedite the reaction kinetics.[27] Although we could not unambiguously identify the individual atomic arrangements of the Cu and Ce atoms at this stage, our microscopy and spectroscopy characterization results strongly suggest that the Cu^+ and Ce^{3+} species are in intimate contact with each other. Therefore, we propose that the active centers of the Cu–Ce/γ-Al_2O_3 catalyst consist of Cu^+–Ce^{3+} complexes and that the Cu and Ce cations work synergistically toward the WGSR (Scheme 1): the Ce^{3+}

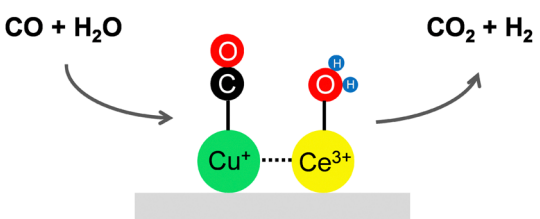

Scheme 1 Schematic diagram illustrating the synergistic effect of the intimate contact between the Cu^+ and Ce^{3+} on the adsorption of the reactant molecules to facilitate the water–gas shift reaction.

adsorbs and dissociates H_2O and the Cu^+ adsorbs CO. The close proximity of activated CO and OH species facilitates the formation of intermediates (*e.g.*, carboxyl) and their subsequent decomposition to CO_2 and H_2. We could not rule out the presence of a small amount of Cu_x^+–Ce_y^{3+} species at this stage. Further elaborate synthesis experiments and full catalyst characterizations are needed to provide a fundamental understanding of the atomically dispersed Cu–Ce/γ-Al_2O_3 catalyst systems.

In summary, atomically dispersed Ce and Cu species were grafted onto commercially available γ-Al_2O_3 to fabricate Cu–Ce/γ-Al_2O_3 catalysts. The introduction of atomically dispersed Ce species led to a remarkable enhancement of the WGSR rate. We proposed that the intimate contact between Cu^+ and Ce^{3+} species and their synergistic effect are responsible for the experimentally observed reaction rate enhancement. Although the atomically dispersed Cu–Ce/γ-Al_2O_3 catalyst contained very low levels of the Ce and Cu metals, its performance is comparable to those of the best Cu/CeO_2 catalysts reported in the literature. These findings highlight the synergetic effects among atomically dispersed metal species and open a new route to develop low-cost WGSR catalysts. The catalyst design strategy is general and can be extended to a variety of atomically dispersed catalysts for the transformation of important molecules.

This work was primarily supported by the US National Science Foundation under grant number CHE-1955474 and CHE-2247571. T. W. and N. Y. acknowledge the Singapore Ministry of Education Tier 2 Grant (MOE-T2EP10221-0008) for the financial support. The authors acknowledge the use of facilities within the Eyring Materials Center and the John M. Cowley Center for High Resolution Electron Microscopy at Arizona State University. The authors thank Dr Xianchun Liu for discussions.

Data availability

Data supporting this study are included within the article and/or supporting materials.

Conflicts of interest

There are no conflicts to declare.

Notes and references

1 C. Ratnasamy and J. P. Wagner, *Catal. Rev.*, 2009, **51**, 325–440.
2 Y. Li, Q. Fu and M. Flytzani-Stephanopoulos, *Appl. Catal., B*, 2000, **27**, 179–191.
3 Y. Zhou, A. Chen, J. Ning and W. Shen, *Chin. J. Catal.*, 2020, **41**, 928–937.
4 X. Wang, J. A. Rodriguez, J. C. Hanson, D. Gamarra, A. Martínez-Arias and M. Fernández-García, *J. Phys. Chem. B*, 2006, **110**, 428–434.
5 A. Chen, X. Yu, Y. Zhou, S. Miao, Y. Li, S. Kuld, J. Sehested, J. Liu, T. Aoki, S. Hong, M. F. Camellone, S. Fabris, J. Ning, C. Jin, C. Yang, A. Nefedov, C. Wöll, Y. Wang and W. Shen, *Nat. Catal.*, 2019, **2**, 334–341.
6 J. A. Rodriguez, P. Liu, X. Wang, W. Wen, J. Hanson, J. Hrbek, M. Pérez and J. Evans, *Catal. Today*, 2009, **143**, 45–50.
7 J. Liu, *ACS Catal.*, 2017, **7**, 34–59.
8 J. Lin, A. Wang, B. Qiao, X. Liu, X. Yang, X. Wang, J. Liang, J. Li, J. Liu and T. Zhang, *J. Am. Chem. Soc.*, 2013, **135**, 15314–15317.
9 J. Ning, Y. Zhou and W. Shen, *Sci. China: Chem.*, 2021, **64**, 1103–1110.
10 K. Mudiyanselage, S. D. Senanayake, L. Feria, S. Kundu, A. E. Baber, J. Graciani, A. B. Vidal, S. Agnoli, J. Evans, R. Chang, S. Axnanda, Z. Liu, J. F. Sanz, P. Liu, J. A. Rodriguez and D. J. Stacchiola, *Angew. Chem., Int. Ed.*, 2013, **52**, 5101–5105.
11 A. L. Cámara, S. Chansai, C. Hardacre and A. Martínez-Arias, *Int. J. Hydrogen Energy*, 2014, **39**, 4095–4101.
12 P. C. P. Caldas, J. M. R. Gallo, A. Lopez-Castillo, D. Zanchet and J. M. C. Bueno, *ACS Catal.*, 2017, **7**, 2419–2424.
13 Y. Bu, C. J. Weststrate, J. W. Niemantsverdriet and H. O. A. Fredriksson, *ACS Catal.*, 2016, **6**, 7994–8003.
14 R. Si, J. Raitano, N. Yi, L. Zhang, S.-W. Chan and M. Flytzani-Stephanopoulos, *Catal. Today*, 2012, **180**, 68–80.
15 X. Li, X. I. Pereira-Hernández, Y. Chen, J. Xu, J. Zhao, C.-W. Pao, C.-Y. Fang, J. Zeng, Y. Wang, B. C. Gates and J. Liu, *Nature*, 2022, **611**, 284–288.
16 J. Z. Shyu, K. Otto, W. L. H. Watkins, G. W. Graham, R. K. Belitz and H. S. Gandhi, *J. Catal.*, 1988, **114**, 23–33.
17 H. C. Kwon, Y. Park, J. Y. Park, R. Ryoo, H. Shin and M. Choi, *ACS Catal.*, 2021, **11**, 10767–10777.
18 O. Sodpiban, T. Kessaratikoon, J. Smith, G. Ren, S. Del Gobbo, S. Das, M. Chi, V. D'Elia and B. C. Gates, *ACS Appl. Mater. Interfaces*, 2023, **15**, 55885–55894.
19 K. Khivantsev, H. Pham, M. Engelhard, H. Aleksandrov, L. Kovarik, X. Li, J. Tian, I. Koleva, I. Song, W. Hu, X. Wei, Y. Sun, P. Tran, T. Graham, D. Jiang, D. P. Dean, C. J. Breckner, J. T. Miller, G. Vayssilov, J. Szanyi, A. Datye and Y. Wang, *ChemRxiv*, 2023, preprint, DOI: 10.26434/chemrxiv-2021-spcd9-v3.
20 S. Poulston, P. M. Parlett, P. Stone and M. Bowker, *Surf. Interface Anal.*, 1996, **24**, 811–820.
21 H. Wan, Z. Wang, J. Zhu, X. Li, B. Liu, F. Gao, L. Dong and Y. Chen, *Appl. Catal., B*, 2008, **79**, 254–261.
22 J. Gu, M. Jian, L. Huang, Z. Sun, A. Li, Y. Pan, J. Yang, W. Wen, W. Zhou, Y. Lin, H.-J. Wang, X. Liu, L. Wang, X. Shi, X. Huang, L. Cao, S. Chen, X. Zheng, H. Pan, J. Zhu, S. Wei, W.-X. Li and J. Lu, *Nat. Nanotechnol.*, 2021, **16**, 1141–1149.
23 A. Bensalem, J.-C. Muller, D. Tessier and F. Bozon-Verduraz, *J. Chem. Soc., Faraday Trans.*, 1996, **92**, 3233–3237.
24 W. Tan, S. Xie, X. Wang, J. Xu, Y. Yan, K. Ma, Y. Cai, K. Ye, F. Gao, L. Dong and F. Liu, *ACS Catal.*, 2022, **12**, 12643–12657.
25 F. Amano, S. Suzuki, T. Yamamoto and T. Tanaka, *Appl. Catal., B*, 2006, **64**, 282–289.
26 J. H. Kwak, R. Tonkyn, D. Tran, D. Mei, S. J. Cho, L. Kovarik, J. H. Lee, C. H. F. Peden and J. Szanyi, *ACS Catal.*, 2012, **2**, 1432–1440.
27 B. Yang, H. Yu, X. Jia, Q. Cheng, Y. Ren, B. He and Z. Xiang, *ACS Appl. Mater. Interfaces*, 2023, **15**, 23316–23327.
28 A. Martínez-Arias, R. Cataluña, J. C. Conesa and J. Soria, *J. Phys. Chem. B*, 1998, **102**, 809–817.
29 M. Fernández-García, E. Gómez Rebollo, A. Guerrero Ruiz, J. C. Conesa and J. Soria, *J. Catal.*, 1997, **172**, 146–159.
30 Z. Cui, S. Song, H. Liu, Y. Zhang, F. Gao, T. Ding, Y. Tian, X. Fan and X. Li, *Appl. Catal., B*, 2022, **313**, 121468.
31 N. Zhang, S. Miyazaki, Y. Qian, Y. Jing, T. Toyao and K. Shimizu, *ACS Catal.*, 2023, **13**, 8503–8515.
32 E. Shaaban and G. Li, *Commun. Chem.*, 2022, **5**, 32.
33 C. Chen, H. Ren, Y. He, Y. Zhan, C. Au, Y. Luo, X. Lin, S. Liang and L. Jiang, *ChemCatChem*, 2020, **12**, 4672–4679.
34 F. Shen, Z. Zhang, Z. Wang, H. Ren, X. Liang, Z. Cai, S. Yang, G. Sun, Y. Cao, X. Yang, M. Hu, Z. Hao and K. Zhou, *Nat. Commun.*, 2024, **15**, 448.
35 R. Zhou, Y. Yang, S. Pande, B. Qu, D. Li and X. C. Zeng, *Phys. Chem. Chem. Phys.*, 2019, **21**, 4006–4014.

